Metal- and hydrogen-bonding competition during water absorption on Pd(111) and Ru(0001)

Mouslim Tatarkhanov,[1,2] D.Frank Ogletree,[1] Franck Rose[1], Toshiyuki Mitsui,[1]

Evgeny Fomin,[1,2] Mark Rose,[1,2] Jorge I. Cerdá[3] and

Miquel Salmeron[1,4*]

[1]Materials Science Division of the Lawrence Berkeley National Laboratory, Berkeley CA, USA.

[2]Department of Physics. University of California Berkeley, CA. USA

[3] Instituto de Ciencia de Materiales de Madrid, ICMM-CSIC, Cantoblanco, 28049 Madrid. Spain

[4]Materials Science and Engineering Department, University of California Berkeley, CA. USA

mbsalmeron@lbl.gov

Abstract

The initial stages of water adsorption on the Pd(111) and Ru(0001) surfaces have been investigated experimentally by Scanning Tunneling Microscopy in the temperature range between 40 K and 130 K, and theoretically with Density Functional Theory (DFT) total energy calculations and STM image simulations. Below 125 K water dissociation does not occur at any appreciable rate and only molecular films are formed. Film growth starts by the formation of flat hexamer clusters where the molecules bind to the metal substrate through the O-lone pair while making H-bonds with neighboring molecules. As coverage increases, larger networks of linked hexagons are formed with a honeycomb structure, which requires a fraction of the water molecules to have their molecular plane perpendicular to the metal surface with reduced water-metal interaction. Energy minimization favors the growth of networks with limited width. As additional water molecules adsorb on the surface they attach to the periphery of existing islands, where they interact only weakly with the metal substrate. These molecules hop along the periphery of the clusters at intermediate temperatures. At higher temperatures they bind to the metal to continue the honeycomb growth. The water-Ru interaction is significantly stronger than the water-Pd interaction, which is consistent with the greater degree of hydrogen-bonded network formation and reduced water-metal bonding observed on Pd relative to Ru.

1. Introduction

Understanding the molecular scale processes involved in the adsorption of water on metal surfaces is important in the fields of wetting, corrosion, catalysis and electrochemistry. Before 2002 the traditional model of the wetting layer on metal surfaces of hexagonal symmetry (fcc(111) and hcp(0001)) was a puckered honeycomb structure in registry with the surface lattice, similar to the bilayer forming the basal plane of ice, with half of the molecules bound to the substrate through the O atoms and the other half elevated by approximately 1 Å and with one H pointing towards the vacuum.[1,2,3] Scanning Tunneling Microscopy (STM) studies of the water monolayer before that year on Pt(111),[4] Ag(111)[5] and Cu(111),[6] were interpreted in this way. This ice-like bilayer model has been challenged by experiment and theory. For instance, Held and Menzel found by low energy electron diffraction that on Ru(0001) the O atoms should be nearly coplanar.[7,8] This result motivated a theoretical analysis of the energetics of water adsorption by Feibelman[9] who concluded that on Ru the stability of the quasi-planar monolayer could be explained by the dissociation of half of the water molecules into H and OH to maximize both hydrogen bonding and oxygen-metal interactions. This partially dissociated model is also supported by other calculations.[10] For the more noble metals Cu, Pd and Pt, the water molecules remain intact[11] forming nearly coplanar hexagonal structures.[12,13] In these structures the water molecules are alternatively flat and vertical, pointing one H either down to the substrate[14] or up into the vacuum.[15,16]

There is the possibility that many experimental results represent metastable structures separated from the thermodynamically stable one by significant energy barriers. Many surface science studies of water adsorption have indeed been carried out at low temperatures in ultra-high vacuum. Glebov *et al.*[17] have shown that water ordering on Pt(111) is strongly influenced by temperature and deposition rate. Michaelides *et al.*[10] found a substantial activation barrier (~0.5 eV) for water dissociation to the energetically favored partially dissociated phase of H_2O-OH on Ru(0001). The existence of such energy barriers, comparable to the binding energy of the water molecules to the substrate or to other molecules highlights the potential for long lived metastable structures.

In previous reports on the growth and structure of water on Pd(111) we have shown that: (1) individual water molecules adsorb on top sites of the Pd(111) surface[18] bonding through the O atom and with the molecular plane almost parallel to the metal surface;[12] (2) isolated water molecules appear in the STM images as protrusions approximately 0.8 Å high under most tunneling conditions; (3) individual molecules diffuse with an activation energy of 126 ± 7 meV;[19] (4) small clusters consisting of two to four molecules exhibit a much higher diffusion rate than monomers at 40 K;[20] (5) high resolution STM images revealed that water hexamers (six molecules forming a hexagonal ring) are the building blocks of larger clusters with honeycomb structure.[12,19]

Another interesting observation is that at temperatures below approximately 100 K the size of the honeycomb structures is limited to 2 or 3 cells in at least one dimension on both metals. This peculiar growth was rationalized by introducing a set of 2D ice-rules.[12] According to these rules: (a) water molecules bind to the metal through the O atom in a nearly flat geometry, similar to that of isolated molecules; (b) the molecules form a honeycomb network with the molecules inside the cluster donating two H-bonds to neighboring molecules and accepting one. Unlike bulk ice, where 4 H-bonds per molecule result in an indefinite extension of the lattice, the 2-dimensional network with 3 H-bonds per molecule can only be continued for a limited number of cells, terminating when the molecules can no longer follow the rules. Only peripheral molecules donate one H-bond or none.

In the present work we present a detailed account of the growth and structure of water on Pd(111) and on Ru(0001) at temperatures below 125 K, where no dissociation is observed. We show that on both metals water adsorption follows a similar pattern. We also show that additional molecules, attached to the edges of the clusters, are weakly bound to the metal atoms. Only after overcoming an energy barrier do these molecules bind to the metal and extend the honeycomb pattern. This happens with appreciable

rate above approximately 60 K. We performed extensive DFT calculations and STM image simulations that give support and detailed insight into the proposed models, and reveal the driving forces behind the 2D ice rules.

2. Experimental

The experimental UHV set-up has been described in detail previously.[20] It consists of a homemade, variable temperature STM system controlled by RHK electronics that allows for cooling of both tip and sample to the same temperature. Preparation of Pd(111) and Ru(0001) was performed by cycles of ion bombardment, using noble gases (Ar, Ne) at 1000 K (1200 K for Ru) with subsequent flashing to 1100 K for Pd and 1300 K for Ru. For Pd both H_2O and D_2O were used, with no significant differences in the results. For Ru only H_2O was used. In each case the water was ultra-pure grade and purified by pumping over the ice and by freeze-thaw cycles. The vapor was admitted into the chamber through a leak valve and adsorbed on the samples at temperatures below 100 K.

In the STM images a gray or color scale is used to represent tip heights at each of the 512x512 image pixels. The gray scale is chosen such that bright corresponds to the tip being farther away and dark closer to the surface. Actual tips heights are shown in image cross-sections. As it is well known, in STM the tip height variations do not necessarily correspond to the real atomic topography since geometry and electronic structure are convolved in the tunneling process.

3. Theory

We have analyzed the geometry and energetics of various cluster configurations by means of DFT based calculations. The total energy optimizations were performed with the SIESTA[21] code under the Generalized Gradient Approximation (GGA).[22] Our basis set choice and convergence parameters have been explained in detail in other related works.[23] Our main approximations are:

i) Neglect of van der Waals (vdW) forces contributing to molecular adsorption and intermolecular H-bonding. To determine the contribution of vdW interactions we used a semi-empirical parametrization scheme proposed in Ref. 24. Although the refined structures remained qualitatively very similar, the vdW correction overestimates H-bonding, leading to far too contracted and corrugated water clusters, corroborating that the GGA alone is reasonably accurate for the case of water adsorption. In what follows we will not address the vdW corrected results and only show the GGA derived ones.

(ii) Neglect of Basis Set Superposition Error (BSSE) corrections associated to the finite basis set size.[24] We have verified that this is our main source of error in the calculated adsorption energies. We have included the so called counterpoise corrections (CP)[25] to the BSSE by splitting the adsorbed cluster system into 2 subsystems: one for the isolated N molecules cluster and another for the clean metal slab. The adsorption energy for the cluster, E_{ads}, is then given by:

$$E_{ads} = -E_{N+M} + N\,E_{H2O} + E_M + E_{BSSE}$$

where E_{N+M}, E_{H2O} and E_M refer to the total energies of the combined cluster plus metal slab, the isolated water molecule and the clean slab, respectively, each corresponding to their optimized geometries. The BSSE correction, E_{BSSE}, is given by:

$$E_{BSSE} = \Sigma_i(E_i^* - E_i)$$

where the summation is over the 2 subsystems and E_i corresponds to the total energy of i^{th} subsystem, freezing its geometry to that in the optimized cluster plus metal system. E_i^* gives the total energy for the same subsystem but using ghost orbitals for the atoms in the system that are not present in subsystem i. Our results indicate that, as expected, BSSE corrections reduce the adsorption energy and tend to be as large as 0.2 eV/H_2O in large clusters. We have also tested a

different CP approach by splitting the adsorbed system into N+1 subsystems: one for each of the N water molecules plus the metal slab M. However, the BSSE term increased up to 0.3-0.4 eV/H_2O clearly favoring 3D type H-bonding vs. planar bonding within the cluster -i.e. highly buckled hexamers become more stable than flat (or almost flat) hexamers. Since this result is in contrast with other DFT results based on plane wave basis codes[13] we have adopted the first CP scheme throughout this work.

(iii) Neglect of zero-point vibrations, which should have a minor effect on total energy differences when all molecules remain intact.

Under these conditions the computed adsorption energy for an isolated water molecule is 222 meV on Pd(111) and 371 meV on Ru(0001). The results of the BSSE corrected adsorption energies for the various cluster structures considered are summarized in Table I for both metals.

The DFT optimized geometries were then used to perform STM image simulations using the GREEN code[26-31] to compare with the experimentally observed images. The parametrization scheme for the tip-sample Hamiltonian as well as any other calculation parameters in the STM simulations were the same as those employed in previous related work.[32] The simulated images were calculated using a hypothetical fcc W(111) oriented tip in the form of a 10 atom pyramid ending in a single atom. Test calculations for other metallic tips provided very similar results. All topographic images were computed for tunneling parameters I=1 nA and V=+100 mV.

4 Results

4.1 From monomers to hexamers

The first steps of water adsorption on Pd(111) and Ru(0001) at 45 K are illustrated in the STM images of Figures 1 and 2 respectively. The images in Figure 1a show individual water molecules and dimers on Pd, increasing in density and forming aggregates of small clusters (b,c). Each image corresponds to an additional exposure of 10 s to water vapor at 5×10^{-6} Torr. Magnified views showing details of the water clusters are shown in Figure 1d-f. The first clusters formed are dimers, producing spots slightly brighter (higher tunneling probability) than the monomers in the images. The dimers could not be resolved into individual molecules at this temperature. Dimers and trimers can be distinguished by their higher mobility relative to the monomers, as explained in a previous paper.[19] STM movies available in our web site illustrate this effect much more clearly.[33] As the cluster size reaches 5 or more molecules their mobility decreases substantially and only fluctuations in shape are observed. The most stable cluster is the hexamer, consisting of a flat or nearly flat (see discussion) aggregate of 6 water molecules forming a regular hexagon, as shown in the enlarged image in Figure 1e.

With additional water exposure small aggregates of hexamers sharing a side are formed, Figure 1f. The size of these aggregates is always limited to a few units as long as the temperature remains below approximately 60 K. The brighter spots at the bottom of the cluster are due to molecules that are not yet incorporated into the hexagonal structure. They will be discussed in detail in the next section.

A similar growth pattern is observed for water adsorption on Ru(0001) for exposures at 45 K, as shown in the images of Figure 2. The first image (a) corresponds to the surface before exposure. Limited-size clusters consisting of one or a few hexamers are observed with a density that increases with water exposure. It is interesting to notice the role of surface imperfections, such as steps and locally strained regions in the adsorption process. One particular example of strain is caused by lattice distortions due to subsurface noble gas atoms implanted during the sputtering process to clean the surface. These atoms aggregate to form 2-dimensional noble-gas "bubbles", a phenomenon already described by other authors.[34] Figure 2a shows such bubbles in the Ru surface before water adsorption. The bubbles appear as round bumps of 40 to 100Å in diameter and about 1 to 2 Å in height. We found that water clusters self-assemble preferentially on the bubbles, as shown in the brighter patches in Figure 2b and 2c. Notice

also the existence of a region around the bubbles devoid of molecules due to capture of the water molecules by the bubbles during growth. With further exposure the clusters cover most of the terrace. Except for this example, the experiments described below were performed on surfaces without bubbles. Another interesting effect of surface topology on water adsorption can be observed at atomic steps. Water forms linear chains parallel to the step edges, as shown in Figure 2 (c) and (d) for Ru(0001). Similar step-edge water absorption was also observed for Pd(111).

4.2 From hexamers to honeycomb clusters and stripes

As shown above, initially water grows in the form of small clusters consisting of a few hexagons. With increasing exposure the density of clusters increases. On Pd elongated stripes of side-sharing hexamers, are formed, as shown in Figure 3a, acquired at 45 K. On Ru below 60 K the growth is in the form of small clusters, as in Figure 4. Extended rows of linked hexamers, similar to those formed on Pd, are observed above that temperature.[35] The internal structure of the clusters is a honeycomb with a $\sqrt{3}x\sqrt{3}$ $R30^{o}$ registry relative to the metal substrate. This can be seen from the dimensions and orientation of the clusters in comparison with atomically resolved images of the Pd substrate. The exact registry of the honeycomb structure relative to the metal atoms is difficult to obtain experimentally. This is due to the large difference in corrugation, around 100 pm for water and 2-3 pm for Pd and Ru, which makes it difficult to resolve both the water structures and the (111) metal lattice corrugation under the same STM imaging conditions.

Cluster growth occurs by attachment of molecules to the edges of the clusters. Below approximately 60 K, these additional water molecules can be observed as bright spots attached to external vertices of the hexagons. They are H-bonded to peripheral molecules, with only weak interaction with the substrate metal atoms, as discussed below. Their apparent heights are 1.7 Å for Pd and 1.1 Å for Ru, and for that reason we will refer to them as "high lying" molecules. These molecules can be found at contiguous or alternating corners of the periphery and in opposite corners of hexamers, as shown in the expanded views in Figure 3b and 3c, for Pd(111), and in Figure 4 for Ru(0001). Edge molecules were observed to hop around the periphery of Ru hexamers at a rate of roughly 1-2 hops per minute at 45 K, as shown in the sequence of images in Figure 4, acquired 1 minute apart. As they hop, the high lying molecules visit all the hexamer corners without any noticeable preference indicating that all sites in the hexamer have similar geometries. From the observed rate we estimate the activation energy for hopping to be around 0.15 eV. Similar edge-molecule diffusion was observed for Pd, however the energetics were not investigated. The number of bright high-lying molecules was conserved during this edge-diffusion process on both metals, implying that the activation energies for either desorption of edge molecules from the cluster or integration into the hexagonal network is significantly higher.

4.3 Cluster growth and structure above 80K

High lying molecules are no longer observed above 80K on Pd, instead all molecules are incorporated into closed hexagonal networks. This result indicates that these molecules are metastable, and heating above 80 K allows them to overcome the activation barrier to bind to other molecules and to the metal substrate extending the honeycomb network. This involves a concerted motion since three to four edge molecules are required to add a hexagonal ring to an existing network. On Ru, heating above 100 K also causes the edge molecules to disappear while at the same time stripes or linked hexagons form. Examples of clusters formed on Pd after heating to 100 K are shown in the images of figure 5. Particularly stable motifs are found, which we labeled "rosettes", made of 7 hexagons, Figure 5b, and "laces", Figure 5c. The later are formed by networks of hexagons enclosing vacancies to accommodate non-donor molecules, as discussed below.

The contrast at the periphery of the rosettes and laces is higher than inside the cluster but less than that of the high lying edge molecules found at lower temperature. This is shown more quantitatively in the profiles in Figure 6.

On Pd below 130 K, the addition of water to the surface extends the honeycomb networks which, however, tend to retain a limited width. Similar growth of stripes occurs on Ru but at temperatures between 100 K and 125 K, above which dissociation of water starts to be observed. Eventually, water forms a second layer on top of the honeycomb network, as shown for Pd in Figures 7a and b.

4.4 From stripes to extended domains

Further increase in temperature, up to 130 K in a background pressure of 10^{-8} Torr of H_2O, resulted in a substantial increase in the lateral size of the clusters. The narrow stripes (2-3 hexagonal units wide), observed at lower temperature, give rise to more extended structures, still retaining the honeycomb $\sqrt{3}\times\sqrt{3}$ R30 periodicity relative to the substrate. Examples of this are shown in Figure 8.

Heating to 130K did not result in dissociation of water on Pd. However, on Ru dissociation has been reported by many authors[36-39] and is also observed in our experiments.[32] We will not discuss the evolution of the water structures on either metal at these higher temperatures in this paper.

5. **Discussion**

The intricate structures formed during low-temperature water absorption on Ru and Pd result from a competition between water-metal interaction and hydrogen bonding. The overall trends can be rationalized by what we call 2-D ice rules.[12] These rules state that water adopts geometries that maximize O-bonding to the metal and H-bonding to neighboring molecules. The models shown in Figure 9 illustrate cluster shapes that can be built following the rules. The rules lead naturally to the formation of the elongated stripes observed experimentally. We now discuss in more detail and with the help of total energy calculations the various bonding configurations involved in the 2-D ice rules.

When a water molecule accepts more H bonds than it donates, the oxygen-metal interaction is significantly altered. This was first shown theoretically for the water dimer,[40] where the H-donating molecule has a reduced oxygen-metal bond length while the molecule accepting the H is raised ~ 50 pm above the surface and has very little interaction with the metal. When a water hexamer is formed, each molecule donates and accepts one H-bond. The molecules are stabilized by ~0.2 eV when they form a complete hexamer compared to the dimer,[12,40-42] making hexamer rings the most energetically favorable surface units. If a water molecule accepts two H bonds from other molecules bound to the metal surface, then it will not interact significantly with the metal due to steric hindrance and also due to competition for the oxygen lone pair electrons which are involved both in accepting H bonds and in water-metal bonding. The plane of these molecules is nearly vertical to the surface, with one H atom between the O and the metal surface.

In the ground-state hexamer, each molecule is in a donor-acceptor-metal (DAM) configuration, both accepting a H bond and interacting with the metal. When hexagons are linked together to form honeycomb structures, or when high lying molecules are attached to hexagons, the vertex molecules participate in three hydrogen bonds and must have either double-donor-acceptor-metal (DDAM) or donor-double-acceptor (DAA) configurations. In addition, at least one molecule per added ring must be in a double-acceptor (AA) or DAA configuration in order to satisfy bond-counting constraints. DFT calculations, described in detail below, have shown that: (1) rings with AA molecules are destabilized, (2) DAA vertices are less stable than DDAM vertices, favoring honeycomb structures with AA molecules on the periphery to those with DAA molecules in the interior, and (3) high lying edge molecules accept H-bonds from ring molecules and are significantly (Ru) or slightly (Pd) more stable bound to DDA molecules than to DAA molecules.

The narrow and elongated structures are therefore the result of energy optimization, as they minimize the number of peripheral AA molecules while avoiding internal DAA vertex molecules. As discussed

below, these AA molecules destabilize the structure by around 0.01 eV for Pd and 0.03 eV for Ru per molecule, and internal DAA molecules further destabilize the structure relative to peripheral AA molecules. This growth mode limits structures to narrow stripes and rosettes no more than three hexagons wide, since internal hexagons must be adjacent to peripheral hexagons. It also drives the formation of internal voids as shown in Figures 5a and 8b.

We report in Table I the calculated adsorption energies per H_2O molecule for the different clusters studied in this work, with monomer and dimer adsorption energies calculated under the same assumptions for comparison. Water clusters adsorb more strongly on Ru than Pd by ~0.1 eV, varying somewhat with cluster size. As explained below, this significant increase in the water-Ru interaction relative to the water-Pd interaction accounts for the differences observed in cluster and network formation on the two metals.

5.1 Flat, buckled and defective hexamers

We considered three initial hexamer configurations, shown in Figure 10a. The first (left) is the most stable structure where all molecules are coplanar and equivalent, and each molecule is bound to a metal atom through the O, accepts one H-bond and donates one H-bond to its neighbors (DAM configuration). In the second (center), the plane of one molecule is rotated so that it becomes perpendicular to the metal surface and accepts two H-bonds (AA configuration). This forces another molecule to be in the DDM configuration to maintain H-bonding (the one in the opposite vertex in the figure), and the remaining molecules are DAM. The third configuration (right) has two vertical AA molecules with one DDM molecule between them, and another DDM and two DAM molecules to complete the ring. The vertical AA molecules in the "defective" hexamers were introduced to explore the stability of the flat hexamer and to gain insight into the energy cost of joining hexamers to form the honeycomb structures which, as discussed above, requires at least one vertical molecule per additional hexamer. It will also be useful in analyzing the bonding of the edge molecules.

We found that upon relaxation each configuration led to different relative minima, with qualitatively very similar optimized structures for the two metals. The DFT calculations show a clear difference between Ru and Pd. Introducing one AA defect destabilizes the hexamer by a sizable 0.03 eV/H_2O on Ru, similar to the results obtained by Haq et al.,[38] while for Pd this energy change is smaller (0.01 eV/H_2O). Introducing a second AA defect further destabilizes the hexamers by an additional 0.03 eV/H_2O on Ru and by 0.17 eV/H_2O on Pd. Defect AA molecules considerably distort the hexamer structure; on Pd (Ru) the oxygen atoms in the DAM molecules are 2.6 Å (2.5 Å) above the metal surface, in the DDMs they are 2.3 Å (2.2 Å) -i.e. more strongly bound to the metal- while for the AAs they are 3.0 Å (3.1 Å) -less strongly bound. The simulated topographic images for the three configurations are shown in Fig. 10b for each metal. The flat hexamers appear as hexagonal rings with little molecular contrast, consistent with the experimental images. Furthermore, the calculated apparent heights for the flat-hexamer images were close to 1.1 and 0.6 Å, again in good agreement with the experimental values that vary between 0.4 and 1.2 Å for Pd and between 0.5 and 0.7 Å for Ru. Surprisingly, the simulated topographic images for the defective hexamers were similar to the flat hexamer model in the case of Pd, but they differed considerably for Ru, showing a substantially distorted ring with significantly higher contrast (0.6 Å) for the vertical water molecules - Figure 10c. This uneven contrast was never observed experimentally on single hexamers on Ru. Therefore, our DFT and STM analysis suggests that flat hexamers are the most frequent structures; defect hexamers may occur on Pd but should hardly exist on Ru.

In addition to the flat hexamer, we also considered a slightly buckled hexamer, similar to that proposed by Michaelides et al.[13] In this configuration (not shown in the figures) every other molecule is slightly raised above the average hexamer plane. The flat and the slightly bucked hexamers yielded almost the same total energies (within 10 meV), the later presenting a buckling among alternating oxygen atoms of only 0.1 Å in Pd and an almost negligible 0.03 Å on Ru. The simulated STM images for the flat and

buckled hexamers were also very similar, and do not allow us to distinguish between the two geometries.

5.2 Peripheral edge molecules

Next we investigated the geometry and energetics of peripherally attached (high lying) water molecules. Three initial structural models depicted in Figure 11(a) were considered: water molecules attached to ring molecules in a flat hexamer by single H bonds (left); water molecules attached to vertical molecules by single H bonds (center); and water molecules attached to adjacent ring molecules (one flat, one vertical) by single H bonds with an additional H bond between them (right). During DFT optimization these structures were relaxed to local minima. The flat octamer is more stable than the double-defect octamer by 0.06 eV/H_2O (Pd) and 0.11 eV/H_2O (Ru). The increased defect destabilization for Ru, already evidenced for the hexamers is consistent with the stronger water-metal interaction. The water molecules attached to the flat hexamers relaxed so that their oxygen atoms were significantly higher than those in the ring (by 0.4 Å for Pd and 0.5 Å for Ru) with the dangling hydrogen atoms tilted towards the surface. This geometry is similar to that of the acceptor molecule in the water dimer on Pd(111), where one molecule is attached to the metal atom and the other is lifted by 0.4 Å.[40] Water molecules attached to vertical molecules in defect hexamers ended up lying much higher than the hexamer plane, by around 2.2 Å, as shown in Figure 11(a). The STM simulations corresponding to these DFT optimized geometries are shown in Figures 11b (images) and c (cross-sections along the lines shown in b). Interestingly, although the geometrical structures are quite similar for Pd and Ru, the calculated contrast of the STM images is very different in the flat-octamer case. On Pd the molecules attached to the flat-octamer have lower contrast than those in the ring, while for Ru the contrast is substantially higher (0.6 Å). On the other hand, the 2 defect octamer case showed a marked contrast enhancement for the edge molecules for both metals: 0.6 Å (Pd) and 0.9 Å (Ru).

In the octamer configuration shown at the right of Figure 11(a) the high lying molecules are attached to adjacent flat and vertical ring molecules. In this configuration the two molecules can form a H bond in addition to the H bonds with ring molecules. For Pd this configuration is more stable than the flat octamer by 0.02 eV/H_2O, as the additional H bond more than compensates for the reduced water-metal interaction of the vertical molecule. For Ru, the flat octamer is still the optimum geometry, the destabilization in this case being only 0.03 eV/H_2O compared to 0.11 eV/H_2O for the double-defect case. The STM simulations, shown in Figure 11, predict a significant contrast enhancement of the high lying molecules for both metals. Whereas such large corrugations are experimentally seen at the cluster edges on Pd (Figure 6(a)) they were never observed on Ru.

Figure 12 shows the DFT optimized structure of a 3 hexamer cluster with six high-lying edge molecules on Pd resembling the experimental image of Figure 6a. The model contains the different types of bonding discussed above for the octamer case. Again, the calculated topographic image and profile displayed in the same figure compares well with the experiments corroborating that at low temperature high-lying edge molecules decorate the clusters on Pd and, if adjacent, will H-bond between them. On the contrary, our analysis indicates that on Ru only flat geometries are observed.

To further investigate the metastable nature of the high-lying edge molecules on Pd we performed an annealing simulation for the 2 defect octamer with two high-lying attached molecules. We set an initial temperature of 200 K and slowly cooled the system in 1 fs steps in the Molecular Dynamics (MD) algorithm. The simulations confirmed that the high-lying molecules changed their binding geometry to that of the more stable flat octamer. Figure 13 shows 3 snapshots corresponding to the initial, intermediate and final steps of the simulation. The high-lying molecules first rotated about the O—H bond tilting the hydrogen towards the metal; next the molecule approached the surface, forcing the vertical water molecule in the hexamer to tilt adopting a “down” configuration; the attached molecule ended up with its dangling hydrogen atoms pointing towards the surface. We also note that after the annealing simulation, the “down” molecule in the hexamer ring left an AA molecule with a H atom

pointing towards the surface inside the octamer. Although the MD simulation was stopped at this point due to computation time constraints, it is likely that H-bonding within the ring will eventually be rearranged, eliminating the "down" molecule in favor of the most stable flat octamer configuration.

The mobility of the attached molecules, shown by their hoping around the hexamer periphery (Figure 4) without separating from it, is remarkable. These molecules are bound by accepting a H-bond from a peripheral ring molecule. The breaking of this bond would lead to the loss of the molecule from the cluster, which was not observed. The hoping mechanism therefore must involve angular distortions of the donor molecule and a neighboring ring molecule in opposite directions. This would bring the attached molecule close to the neighboring corner where it can accept a new-H bond while breaking the one with the original molecule. In other words, there must be a substantial amount of flexibility in the H-bonding.

5.3 Extended Chains

DFT calculations were carried out for three possible geometries of an extended chain two hexagonal rings wide on Ru(0001). Each additional linked hexagon adds from three to four water molecules to the chain and, as described above, each ring must have at least one double-acceptor vertical molecule to satisfy bond counting. Figure 14 shows the calculated geometries. The left panel is the favored geometry, with all the molecules at internal vertices in DDA configurations, and with a defect (AA) peripheral molecule in each ring with H-down. In the other two calculated geometries, the peripheral molecules are DA and two of the four internal vertices are DAA, either with the dangling H atom down toward the Ru surface (center), or up to vacuum (right). Having the double acceptor molecule at the periphery is favored by 0.03 eV per defect relative to the H-up internal DAA defect and by 0.15 eV per defect relative to the H-down geometry. A similar trend is expected for the Pd(111) case (not calculated). Since single AA molecules in isolated hexamers have a modest energy cost, the destabilization due to peripheral AA molecules in extended networks is probably also modest. Internal DAA vertices disrupt the H-bonding network in Ru, and are likely to do the same on Pd, similar to the double-defect hexamer case.

These results explain the limited width of the lace-like honeycomb structures. As structures extend, the vertical AA molecules are pushed to the periphery, where they limit the attachment of either single high-lying molecules (energy cost 0.2 to 0.3 eV relative to flat ring molecules) or additional hexagonal rings (cost ~0.03 eV per embedded double-acceptor). Larger islands with embedded AA molecules are only formed by dosing at sample temperatures above near 140 K, where the water desorption rate is already significant. Extended two-dimensional honeycomb islands approach the limit of one half DDA and one half DAA molecules, compared to the extended double chains, with one third AA and two thirds DDA molecules, or extended single chains, with one quarter AA and three-quarters DA or DDA molecules.

6. Summary and conclusions

We have presented a detailed study of the growth pattern of water on Pd(111) and Ru(0001) in the monolayer regime at temperatures below 130 K and shown many similarities between the two metals. At these temperatures no dissociation of water occurs. We have shown that growth proceeds by first formation of hexamers, the most stable cluster of water. This cluster is made of flat lying molecules, making O-covalent bonds with the substrate and inter-connected by H-bonds. The other H is dangling at the edge of the cluster.

We have shown that 2-dimensional ice rules, requiring maximization of both H-bonding and O-metal bonding, combined with the greater stability of peripheral AA molecules to internal DAA molecules, explain the peculiar growth pattern of water in the form of elongated stripes of honeycomb structures 1

to 3 cells wide. The growth of more extensive structures requires the incorporation of additional double-acceptor vertically-oriented defect molecules. The stronger tendency to form extended hexagonal networks on Pd relative to Ru is consistent with the relatively weaker water-metal interaction for Pd. With the help of DFT calculations we have obtained considerably new insights and an improved understanding of the structure of intact water on both metals.

The attachment of molecules at the edge of the clusters during growth reveals interesting aspects of the water growth process. We found that water molecules attach to the edges by accepting a H-bond from single-acceptor ring molecules. These edge molecules can hop around corner sites in the periphery even at 50 K and show no preference for attaching to contiguous or alternating corners of the hexagon. Adjacent edge molecules on Pd hexagons can start to form H-bonded connections between molecules which are not interacting with the metal substrate – the first step in the formation of three-dimensional water structures. Again, DFT calculations and Molecular Dynamic simulations have added considerably and deepened our understanding of the growth mechanism of water on metal surfaces.

7. Acknowledgments

This work was supported by the Director, Office of Energy Research, Office of Basic Energy Sciences, Materials Sciences Division, of the U.S. Department of Energy under Contract No. DE-AC02-05CH11231. JC was supported by the Spanish Ministry of Science and Technology under Project No. MAT2007-66719-C03-02.

Table I – Water Cluster Binding Energies

Energies per molecule in eV, relative to gas-phase H_2O, and bond counts for water clusters on Pd and Ru. Where multiple cluster structures have been considered, the most stable energy is in bold.

Cluster	Pd	Ru	H Bonds	Metal Bonds
Isolated monomer	**0.22**	**0.37**	0	1
Isolated dimer	**0.41**	**0.52**	1/2	½
Hexamer, flat	**0.59**	**0.69**	1	1
Hexamer, one AA	0.58	0.66	1	5/6
Hexamer, two AA	0.42	0.62	1	2/3
Flat octamer	0.60	**0.70**	1	3/4
Octamer one defect	**0.62**	0.67	9/8	3/4
Octamer two defects	0.54	0.59	1	1/2
Double-chain edge H-down	*	**0.76**	4/3	2/3
Double-chain internal H-down	*	0.71	4/3	2/3
Double-chain internal H-up	*	0.75	4/3	2/3

* - not calculated

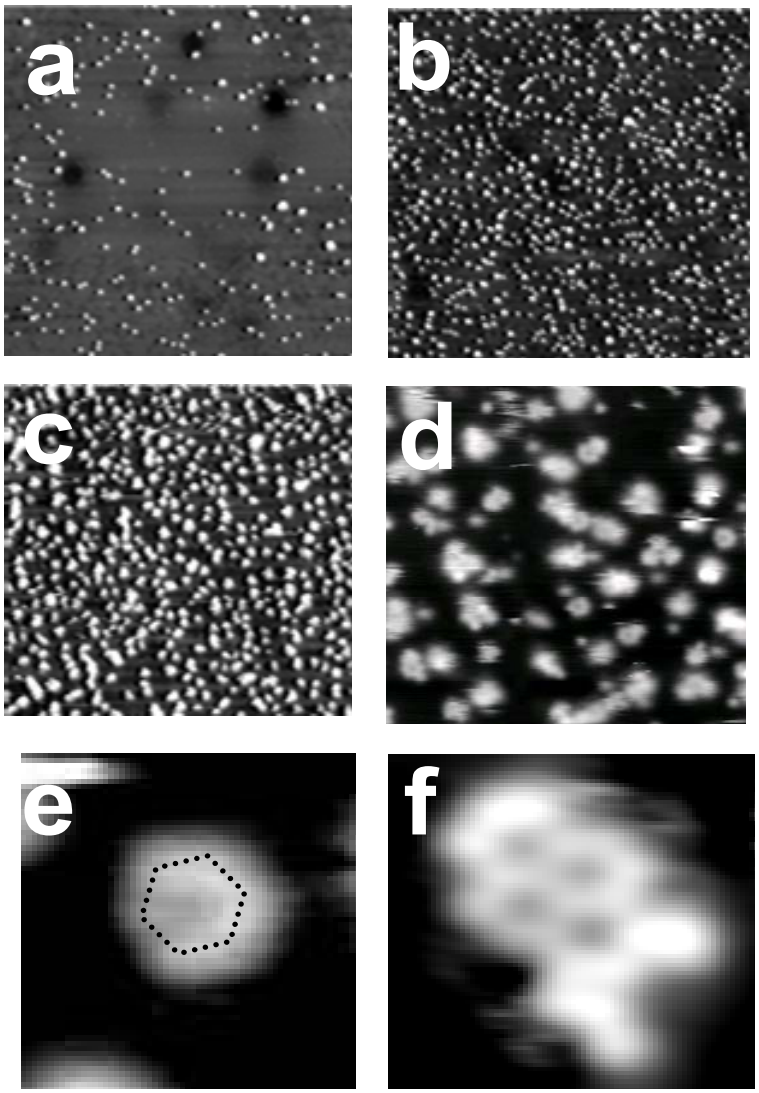

Figure 1. STM images of water molecules on Pd(111) at 45 K. (a)-(c) (60 × 60 nm^2): same region after consecutive exposures of H_2O (10 s at 5 × 10^{-6} Torr). (a) Water monomers. (b) Monomers, dimers and trimers. (c) Small aggregates of up to 10 molecules. (d) Magnified view (10 × 10 nm^2) of (c) showing a mixture of hexamers, monomers and other aggregates. (e) Single hexamer (1.6 × 1.6 nm^2). Hexamers were found to be the most stable water clusters. (f) (2 × 2 nm^2) image showing three hexagons with two additional molecules attached to the corners of the bottom hexagon. Scanning conditions: (a, b) 80 mV, 85 pA; (c) 163 mV, 75 pA; (d,e) 120 mV, 175 pA; (f) 120 mV, 175 pA.

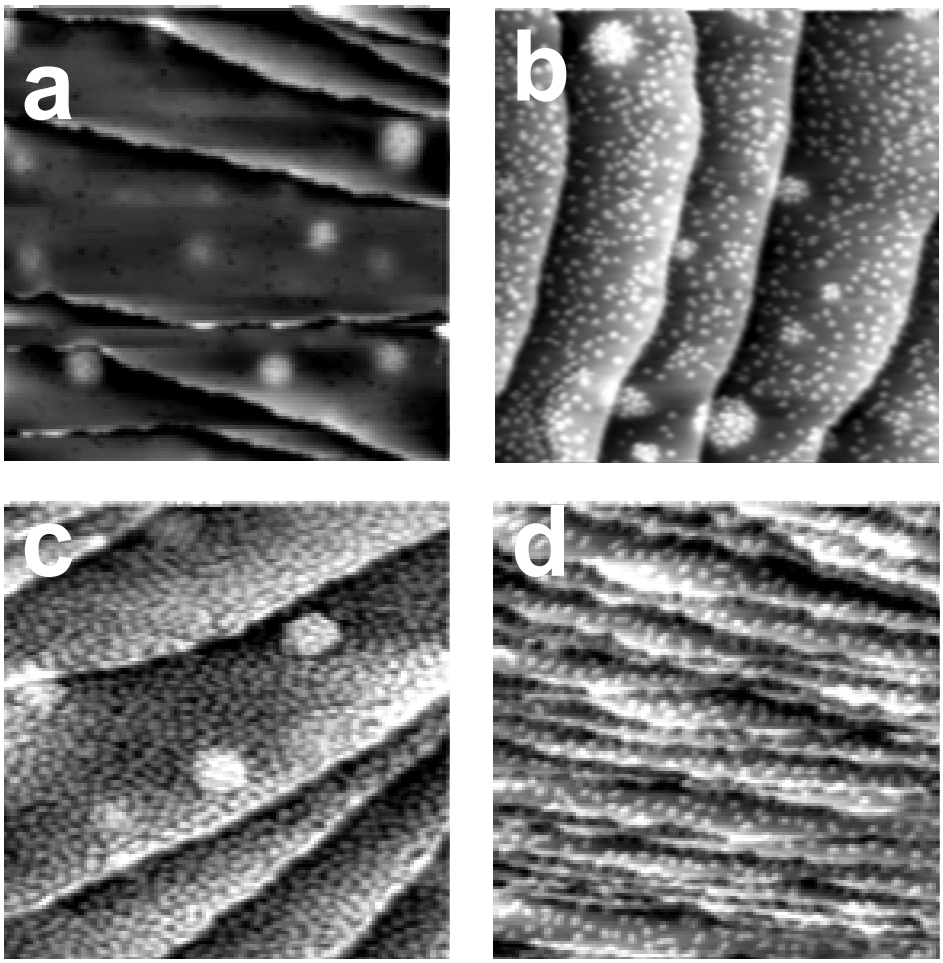

Figure 2. Water clusters on Ru(0001) adsorbed at 45 K. (a) 80 × 80 nm^2 image before water exposure showing steps and terraces. The bright round regions correspond to subsurface noble-gas bubbles generated by sputtering and moderate annealing. (b) 57 × 57 nm^2 image after a water exposure that produced small clusters, each containing roughly 10 to 20 molecules. The water clusters preferentially nucleate on the bubbles, which are surrounded by a region devoid of water due to accretion into the bubble. (c) 80 × 80 nm^2 image obtained after further exposure that increased the density of clusters but not their average size. (d) 70 × 70 nm^2 image of another region of the sample surface showing water clusters confined in narrow terraces and decorating the steps. Scanning conditions: (a) 1.15 V, 150 pA; (b) 110 mV, 370 pA; (c,d) 110 mV, 170 pA.

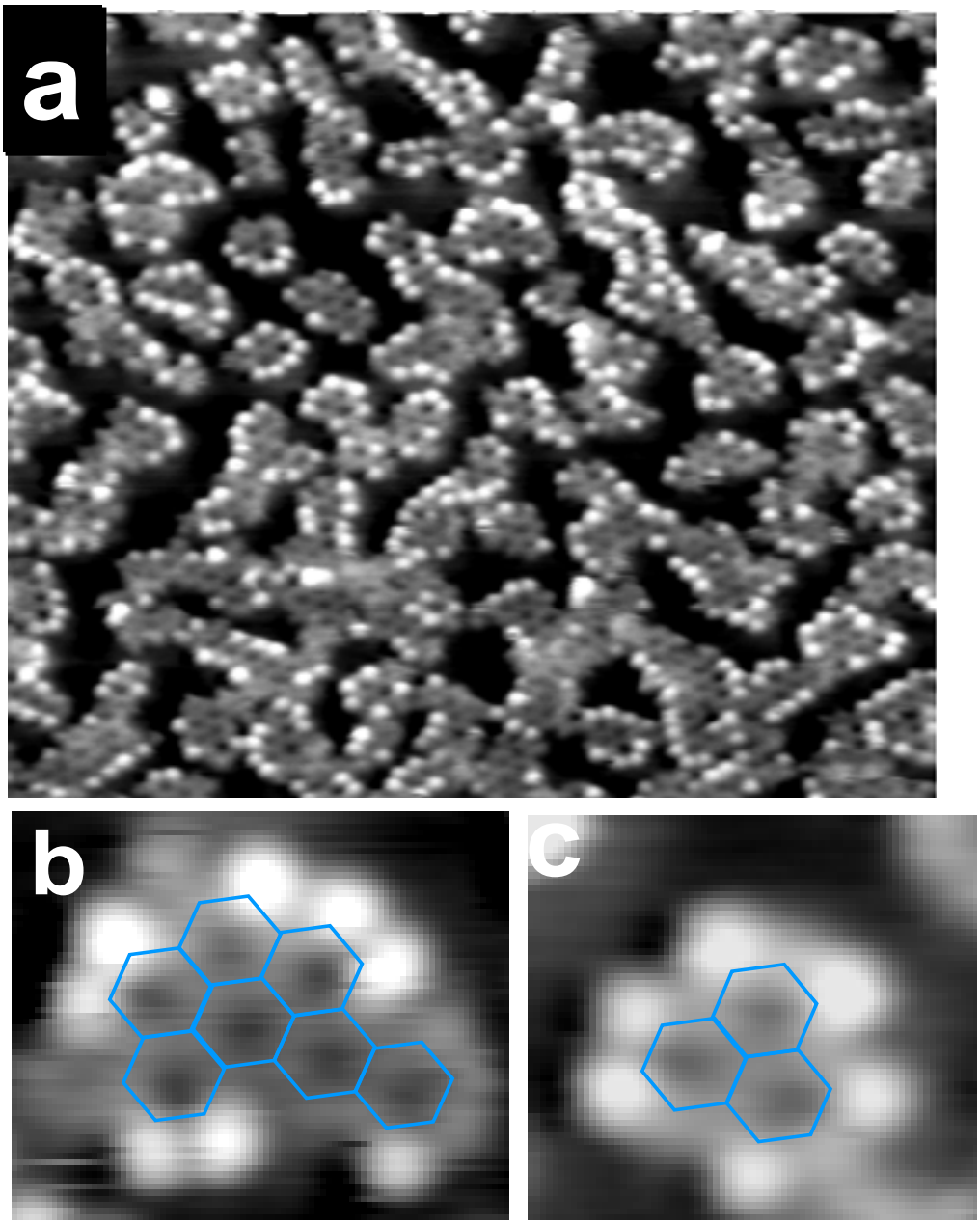

Figure 3. (a) 20 × 20 nm^2 image showing elongated water clusters on Pd(111) at 45 K formed after increasing the water coverage. The clusters have are made of side sharing hexagons forming a honeycomb lattice with a width limited mostly to two or three hexagonal rings. As in Fig. 1f, bright spots correspond to additional water molecules adsorbed at the periphery of the clusters. (b) and (c): expanded views of two clusters in (a) with overlaid hexagons to show the location of the bright spots at the edges. Scanning conditions: 84 mV, 110 pA.

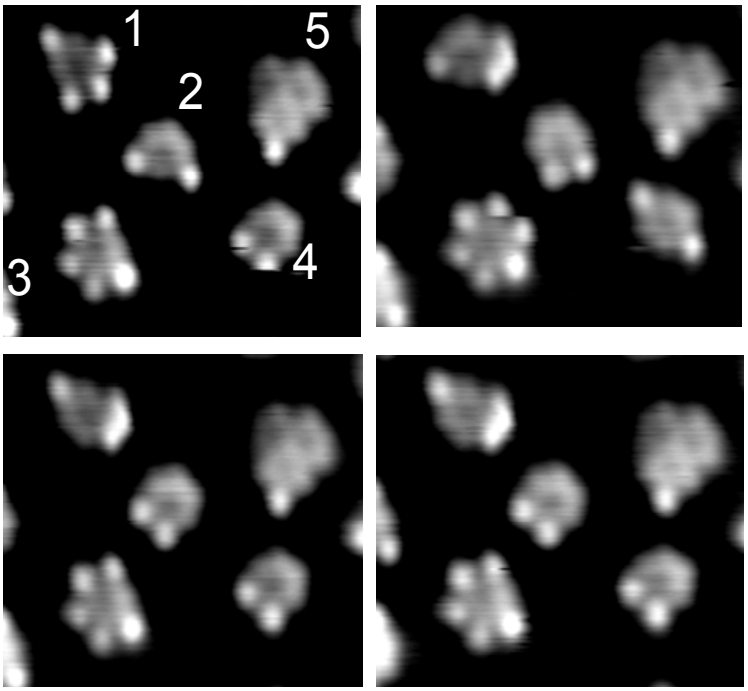

Figure 4. 6.5 × 5.7 nm^2 images of water on Ru(0001) acquired at 50 K at 1 minute intervals. The images show 4 individual hexamers (labeled 1 to 4) and a cluster of three linked hexamers (labeled 5). They have attached water molecules at the edge. Hexamer #1 has 3 attached molecules, #2 and #4 have 2 molecules each, and #3 has 5 molecules. Cluster #5 has one molecule. The attached molecules change their position from one vertex to another with a time constant around 1 minute. In the second frame, #3 appears to have 6 molecules, due to imaging one of the molecules twice during scanning, due to its motion from vertex to vertex. Scanning conditions: 170 mV, 0.7 nA.

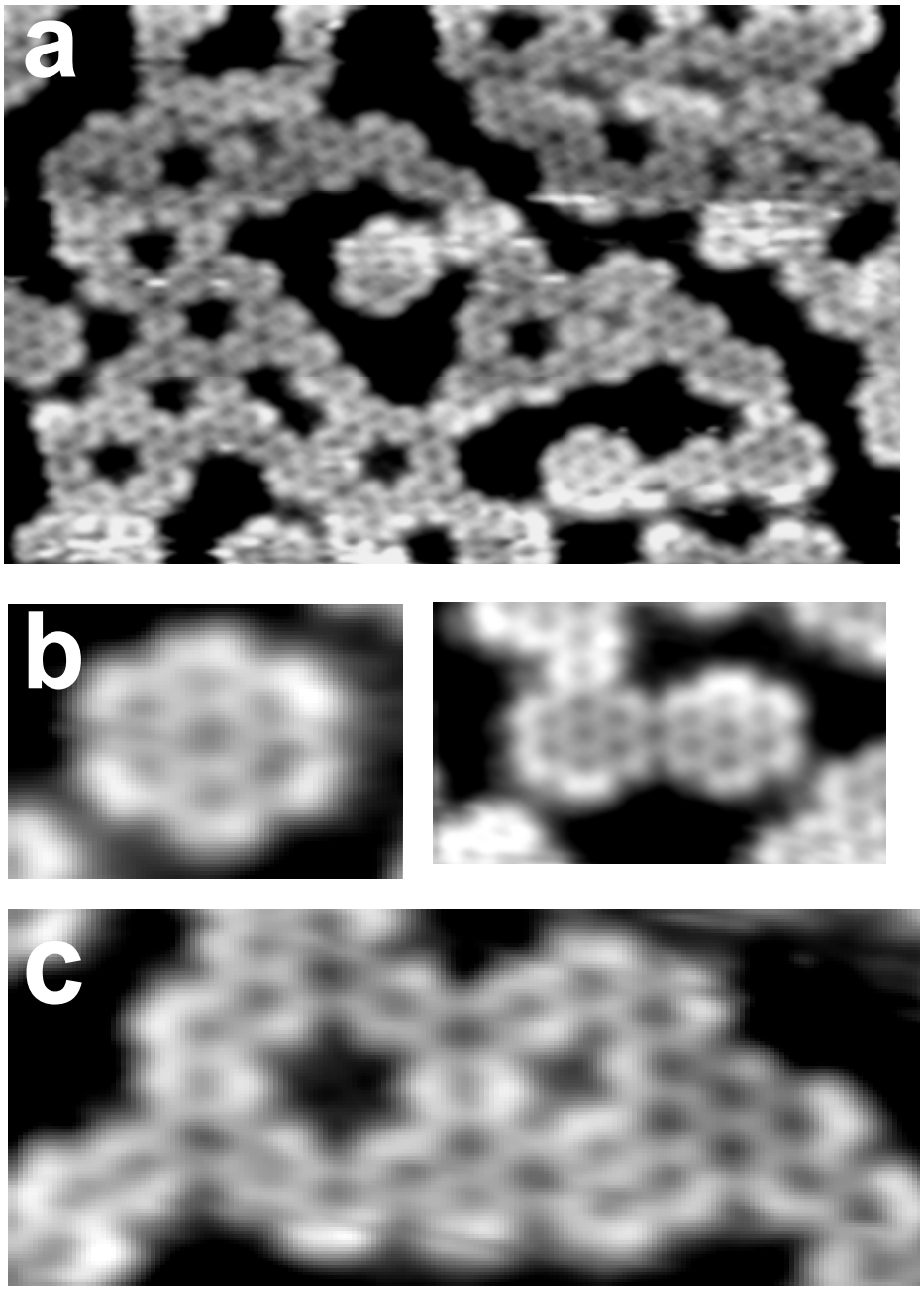

Figure 5. Water structures formed by water adsorbed on Pd(111) after heating to 100 K. (a) Chains of hexagons (10 × 8 nm^2). (b) Expanded view showing "rosette" structures (left, 2.4×2.3 nm^2, right 5.2 × 3.2 nm^2). (c) Lace structure (5.0×2.6 nm^2). The attached molecules (bright protrusions in Fig. 3 and 4) are not observed after annealing above 80 K on Pd, indicating that they are metastable. Scanning conditions: 170 mV, 100 pA.

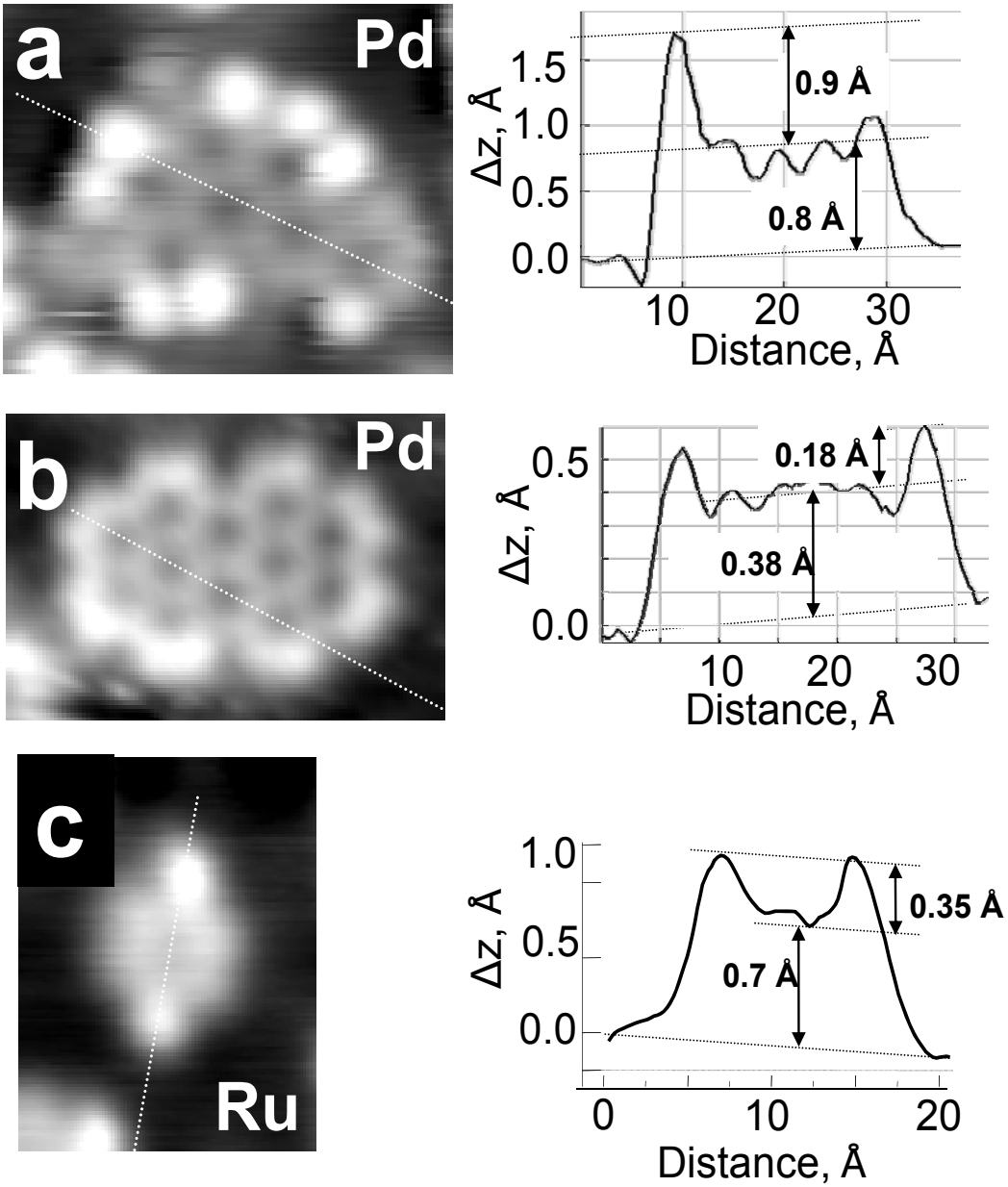

Figure 6. Magnified images of water clusters and corresponding cross-sections. (a) A low temperature cluster on Pd at T<60 K, consisting of 7 hexagons and 8 molecules attached at the periphery. The tip is 0.9 Å higher over these molecules than over the rest of the molecules in the cluster. (b) The clusters formed above 80 K on Pd do not show the high contrast attached molecules at the periphery. The edge molecules contrast is higher (by ~0.2Å) than that of the molecules in the middle of the hexagons. (c) Hexamer on Ru(0001) at 50 K with two attached water molecules. The cross-sections indicates that the apparent height of these molecules is 0.35 Å higher than the rest of the hexamer. Imaging conditions as in Fig. 3, 4 and 5.

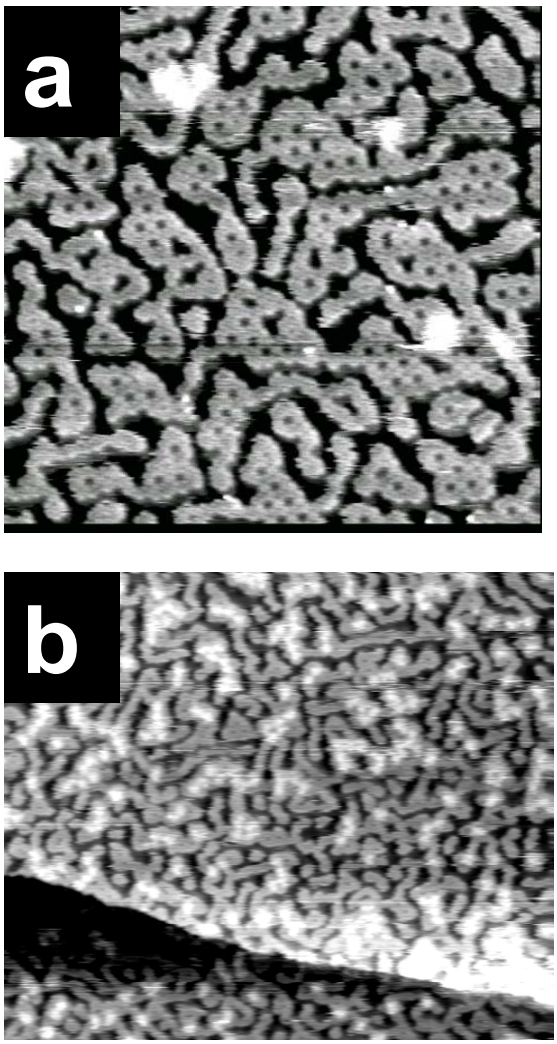

Figure 7. Elongated water clusters formed after additional exposure of water at 110 K on Pd(111). (a) 20 × 20 nm^2 image showing that during growth the stripes remains narrow, filling the space as densely as possible but avoiding coalescence. (b) 30 × 30 nm^2 image obtained after additional exposure to water. A second layer (brighter areas) starts to grow before a full monolayer of water covers completely the substrate. The first layer retains its elongated and narrow structure. Scanning conditions: (a) 0.2 V, 120 pA; (b) 0.17V, pA.

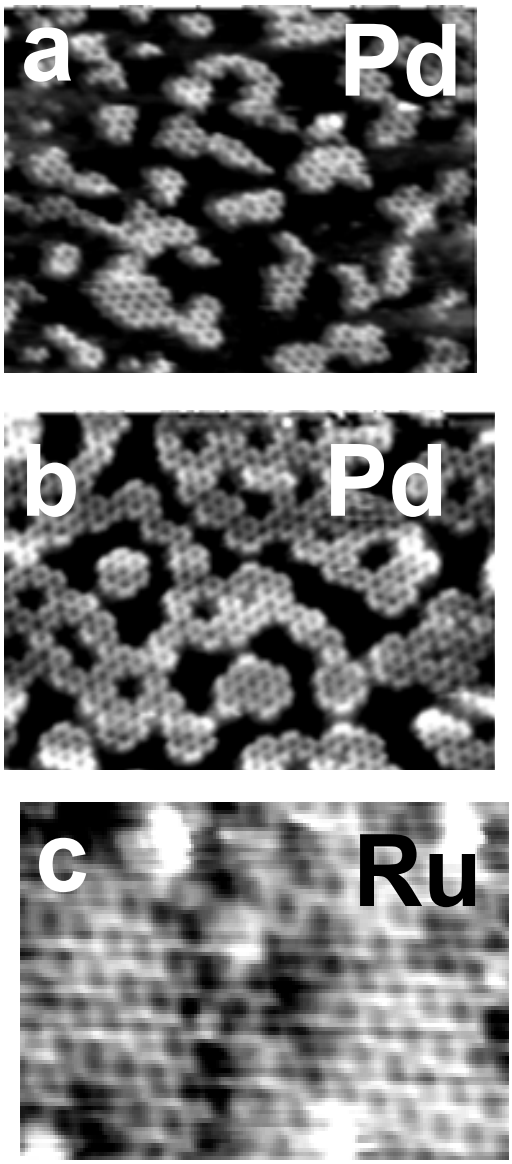

Figure 8. (a) and (b) 10 × 7 nm STM topographic images of water on Pd(111) after heating to 130K showing honeycomb clusters with lateral sizes larger than those formed at lower temperatures (< 130K). (c) 6 × 3 nm topographic image of water on Ru(001) after heating briefly to 130 K also shows extensive honeycomb structures. On this surface heating longer times, or at higher temperature, results in the partial dissociation of a fraction of the water molecules. Scanning conditions: (a,b) 170 mV, 100 pA; (c) 170 mV, 0.7 nA.

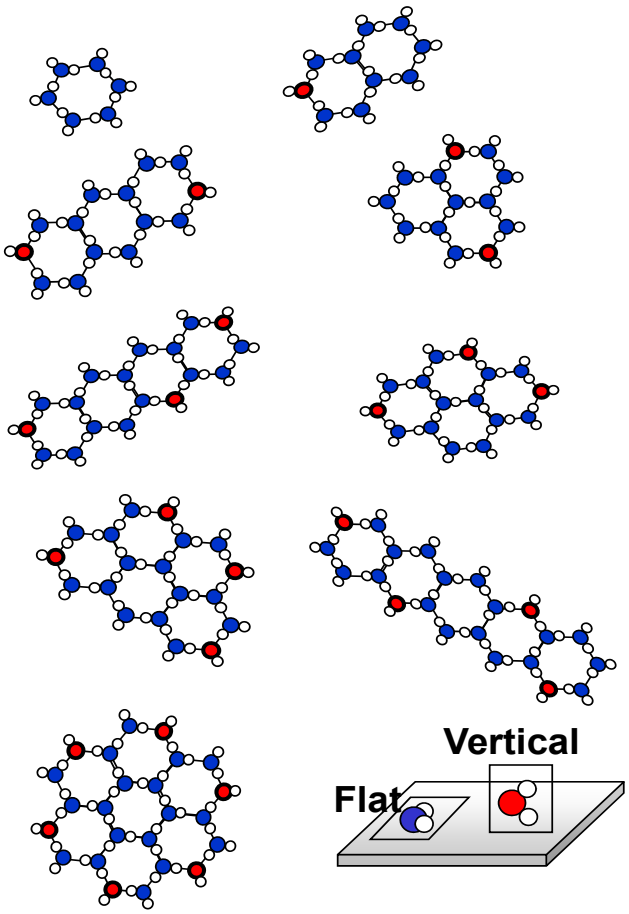

Figure 9. Schematic drawings showing water clusters of side sharing hexagons. The clusters obey so called "2D ice rules". These rules require maximization of O-metal bonding and H bonding to adjacent molecules. Ideally a molecule will donate 1 or 2 H-bonds while accepting one, the maximum H-bonding possible in 2 dimensions (blue colored "flat" molecules parallel to the surface). While in 3D ice this can be continued indefinitely, in 2 dimensions this can only occur in small clusters or narrow stripes. Beyond the hexamer (top left), each additional hexamer must have at least one "defect" molecule of double acceptor nature with its plane nearly vertical to the surface (red colored molecules). Each defect has an energy cost, which is higher at internal vertices than on the cluster periphery. Stripes wider than 3 hexagons, or extended clusters require 2 or 3 defect molecules per hexagon. Minimizing the energy cost of defects gives rise to the observed stripe structures formed by water on Pd(111) and Ru(111) at low temperature.

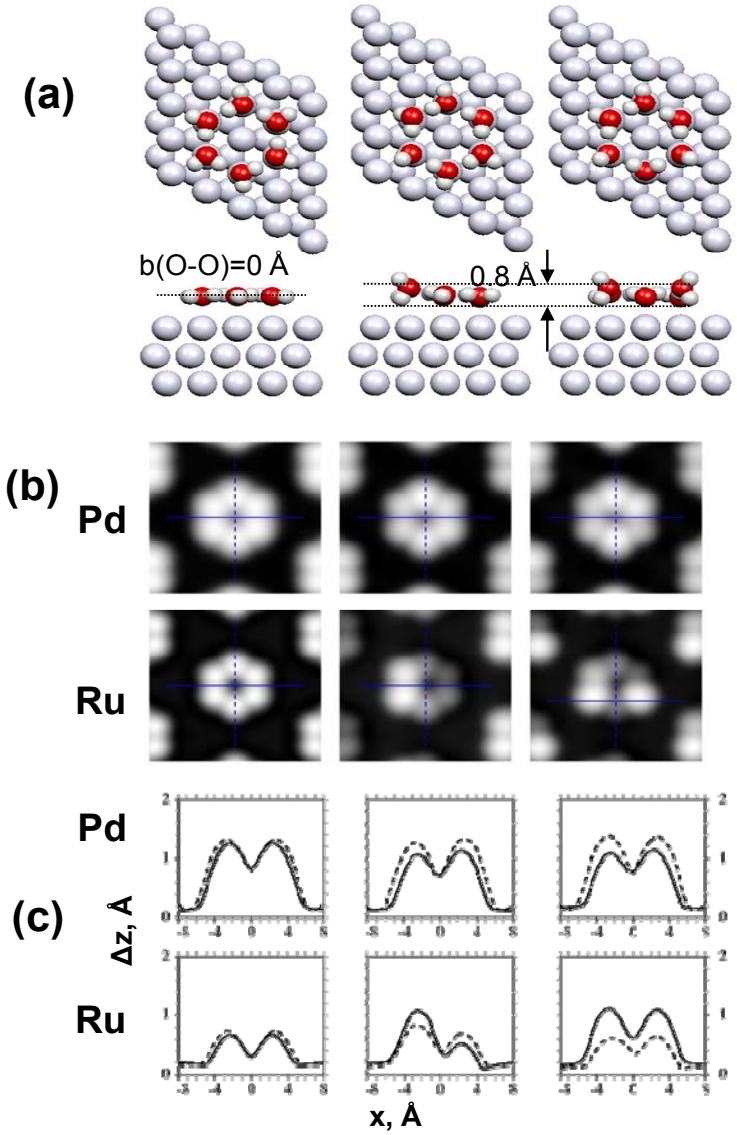

Figure 10. (a) Top and side views of DFT optimized geometries for the three water hexamer structures on Pd(111) and Ru(0001) studied in this work. Left: flat hexamer with coplanar molecules. Each water molecule donates one H-bond and accepts another H-bond with the neighboring molecules and is bound to a metal atom through the O (DAM). Middle: 1 defect hexamer, with four DAM water molecules in a geometry similar to that in the flat hexamer, one defect AA molecule with its plane vertical to the surface, and a flat double-donor (DDM) molecule between two DAM. Right: 2 defect hexamer with two DAM, two DDM and two AA. Oxygen atoms are red, hydrogen white and the metal atoms light gray. (b) Corresponding STM topography simulations calculated with a single atom terminated W(111) oriented tip. Tunneling parameters employed in the simulation are: 100 mV, 1 nA. Only the defect hexamers on Ru shows a sufficiently different calculated contrast to be distinguishable in the experiments. (c) Topographic profiles along the blue lines superimposed in the images in (b). The calculated hexamer corrugation on Pd (1.1 Å) is larger than on Ru (0.7 Å).

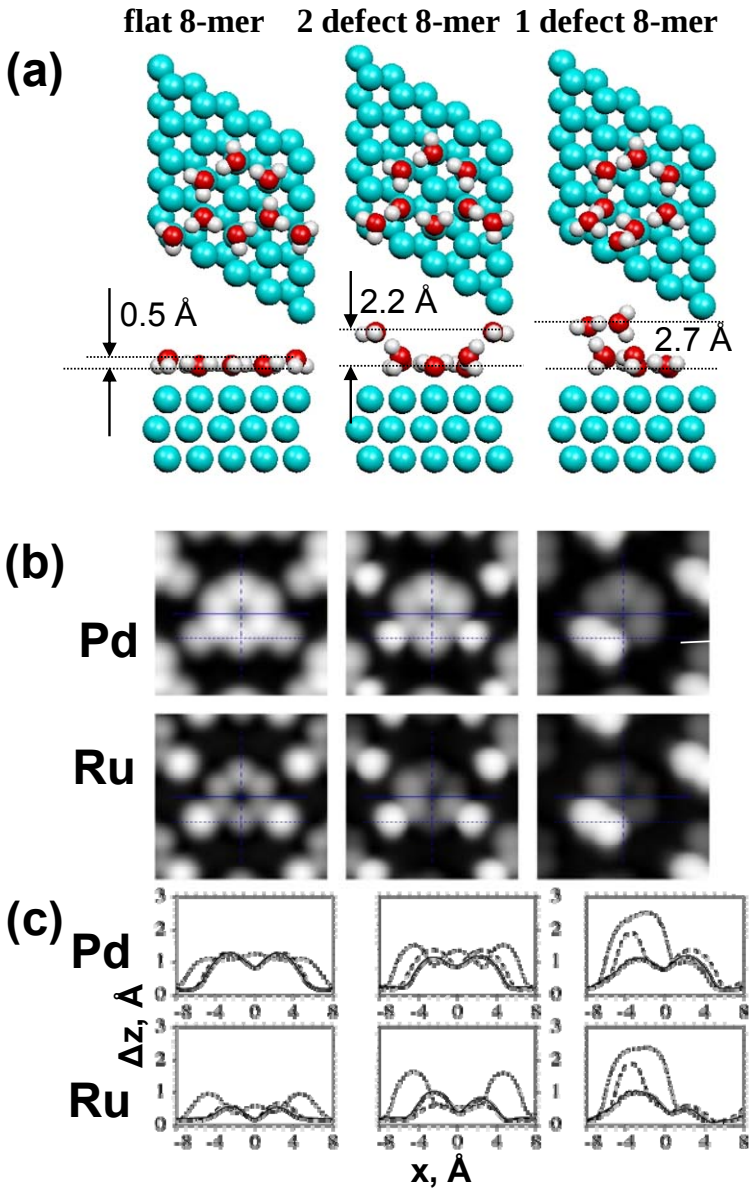

Figure 11. a) Top and side views of the DFT optimized geometries for three water octamer structures on Pd(111) and Ru(0001). Left: flat octamer cluster consisting of a flat hexamer with two attached water molecules acting as H-bond acceptors and with the hydrogen atoms pointing away from the cluster. The attached molecules are raised above the hexamer plane by 0.4 Å and 0.5 Å, for Pd and Ru, respectively. Middle: 2 defect hexamer with two high lying molecules attached to defect AA molecules in the hexamer. Right: 1 defect hexamer with two adjacent attached high-lying molecules H-bonded to each other. (b) Corresponding STM simulations. (c) Topographic profiles along the blue lines superimposed in the images in (b).

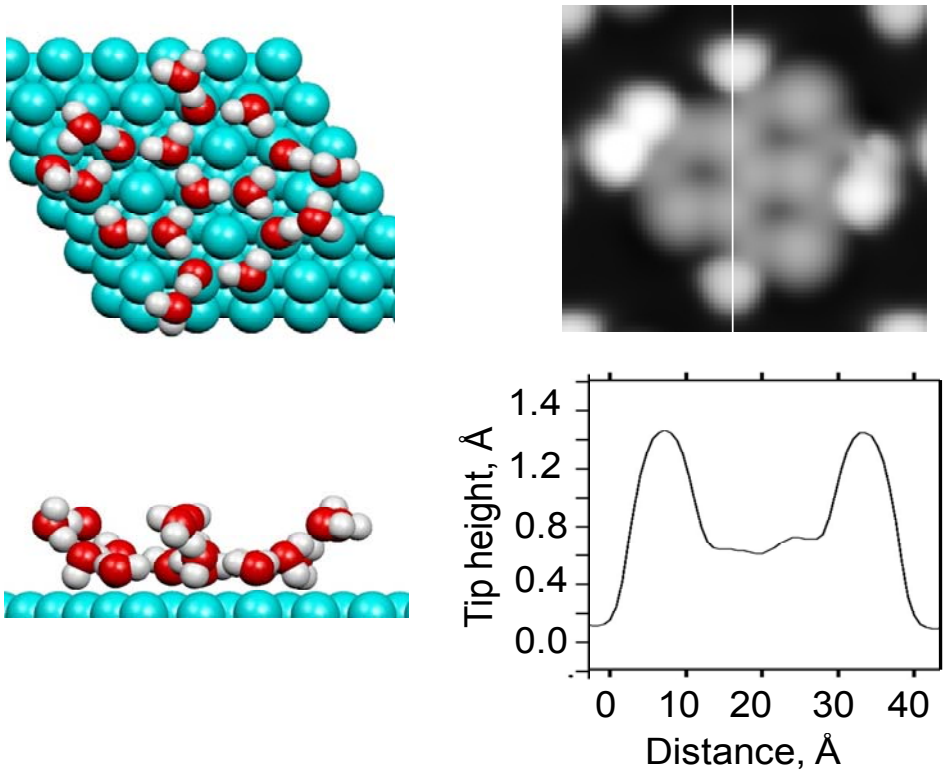

Figure 12. Left: Top and side views of the DFT optimized geometry of a 19 water molecules cluster on Pd(111) forming a three hexagon flat honeycomb cluster with three high lying molecules bound to vertical AA molecules at the edges of the cluster (as in the 2-defect octamer of fig 11) and another pair high lying molecule attached and H-bonded to each other (as in the 1-defect octamer of fig 11). Right: The corresponding STM simulation and topographic profile along the vertical line in the image. The simulated corrugation is in accordance with the experimental profile for similar structures on Pd(111) (as in Fig. 6 (a).

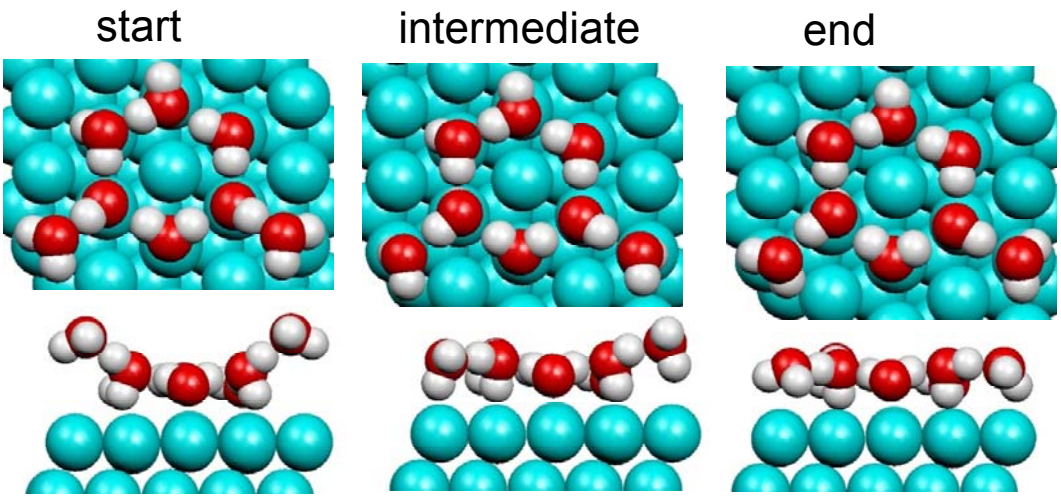

Figure 13. Three snapshots from a Molecular Dynamics simulation at T = 200 K showing the evolution of the 2 defect water octamer on Pd(111) toward a more stable flat structure. The left frame corresponds to the initial geometry, identical to that at the right in Fig. 11(a). The frame in the middle corresponds to an intermediate configuration, with the high lying molecules rotated and shifted closer to the surface. The donor vertical molecule in the hexamer rotates simultaneously adopting a H-down configuration. The frame at the right shows the molecular configuration at the end of the simulation run, with the attached molecules roughly coplanar with the hexamer, similar to the flat octamer in Fig. 11(a), although the defect vertical molecules within the hexamer remain in an H-down configuration.

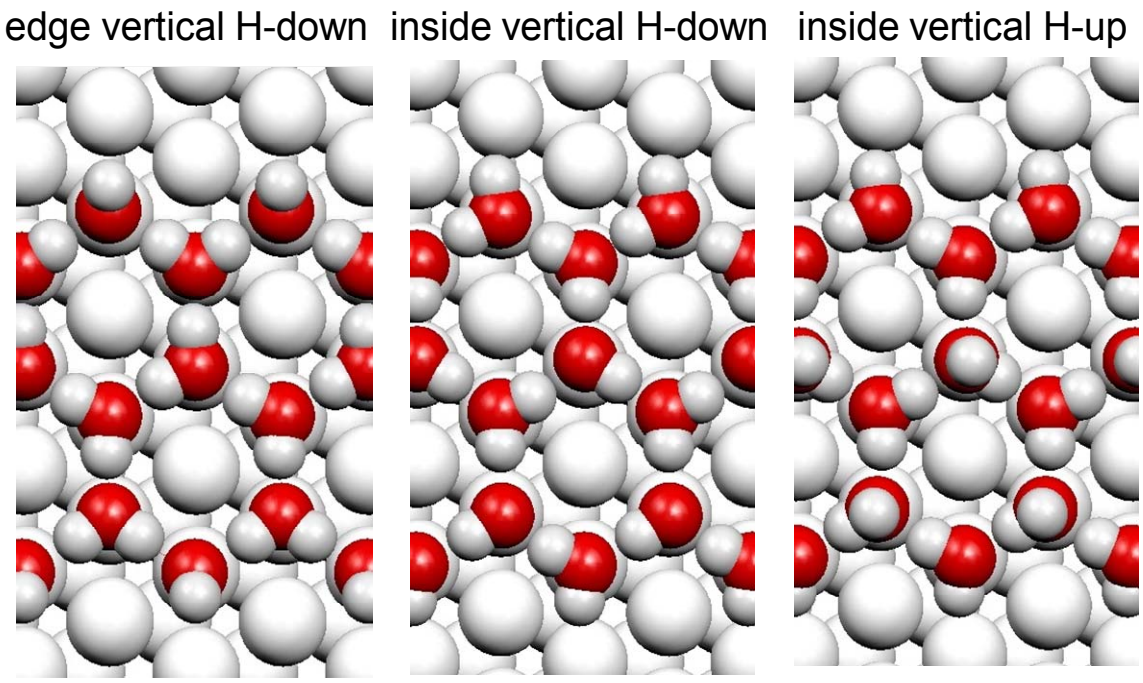

Figure 14. Top views of the DFT optimized geometries for three different extended double-chain "stripe" structures on Ru(0001). They all contain 6 water molecules in the unit cell, out of which 4 are flat and 2 defective (i.e., with their plane vertical) located either at the stripe edges (left), or inside the stripe as H-down (middle) or as H-up (right). The left structure, with the vertical double acceptor molecules at the edge, is the most stable.

References

1. Doering, D.L.; Madey, T.E. *Surf. Sci.***1982**, 123, 305.

2. Thiel, P.A.; Madey, T.E. *Surf. Sci. Rep.***1987**, **7**, 211.

3. Henderson, M. A. *Surf. Sci. Rep.* **2002**, 285, 1-308.

4. Morgenstern, M.; Mueller, J.; Michely, Th.; Comsa, G.; *Z. Phys. Chem.* **1997,** 198, 43.

5. Morgenstern, K.; Nieminen, J.*Phys. Rev. Lett*. **2002**, 88, 66102.

6. Morgenstern, K.; Rieder, K.H. J. *Chem. Phys*. **2002**, 116, 5746.

7. Held, G.; Menzel, D. *Surf. Sci.* **1994,** 316, 92, and **1995**, 327, 301.

8. Puisto, S.R.; Lerotholi, T.J.; Held, G.; Menzel, D. *Surf. Rev. and Lett*. **2003**, 10, 487.

9. Feibelman, P.J. *Science.* **2002**, 295, 99.

10. Michaelides, A.; Alavi, A.; King, D.A.; *J. Am. Chem. Soc.* **2003**, 125, 2746.

11. Michaelides, A.; Alavi, A.;. King, D.A. *Phys. Rev. B*. **2004**, 69, 113404.

12. Cerda, J.; Michaelides, A.; Bocquet, M. L.; Feibelman, P.J.; Mitsui, T.; Rose, M.; Fomin, E.; Salmeron, M. *Phys. Rev. Lett.* **2004,** 93, 11.

13. Michaelides, A.; Morgenstern, K. *Nature,* **2007**, 6 , 597.

14. Ogasawara, H.; Brena, B.; Nordlund, D.; Nyberg, M.; Pelmenschikov, A.; Petterson, L.G.M.; Nilsson, A. *PRL*, **2002,** 89, 27 .

15. Pache, T.; Steinruck, H.P.; Huber, W.; Menzel, D. *Surf. Sci.* **1989**, 224, 195-214.

16. Beniya, A.; Yamamoto, S.; Mukai, K.; Yamashita, Y.; Yoshinobu, J. *JCP,* **2006**, 25, 054717.

17. Glebov, A.; Grahm, A. P.; Menzel, A.; Toennies, J.P. *J. Chem. Phys.* **1997**, 106, 9382.

18. Fomin, E.; Tatarkhanov, M.; Mitsui, T.;. Rose, M.; Ogletree, D.F.; Salmeron, M. *Surf. Sci.* **2006**,600.

19. Mitsui, T.; Rose, M.K.; Fomin, E.; Ogletree, D. F.; Salmeron, M. *Science*, **2002**, 297.

20. Behler, S.; Rose, M.K.; Dunphy, J.C.; Ogletree, D.F.; Salmeron, M.; Chapelier, C. *Rev. Sci. Instrum.* **1997**, 68, 2479. The current STM has a modified scanner enclosed in a copper shield clamped to the sample stage so that tip and sample are at the same temperature.

21. Soler, J.M.; Artacho, E.; Gale, J.; García, A.; Junquera, J.; Ordejón, P.; Sánchez-Portal, D.; *J. Phys. Condens. Matter.* **2002,** 14, 2745. Details of the DFT calculations can be reviewed in Ref. 27.

22. Perdew, J.P.; Chevary, J.A.; Vosko, S.H.; Jackson, K.A.; Pederson, M.R.; Singh, D.J.; Fiolhais, C.; *Phys. Rev. B,* **1992**, 46, 6671.

23. Hamann, D.R. *Phys. Rev. B,* **1997,** 55 ,R10157.

24. Ortmann ; Bechstedt, F. *Phys. Rev. B.* **2006**, 73, 205101.

25. Hobbs, C; Kantorovich, L.; Gale, J.D. *Surf. Sci.* **2005**, 591, 45.

26. Boys, S.; Bernardi, F. *Mol. Phys*. **1970,** 19, 553.

27. Cerdá, J.; Van Hove,M.A. ; Sautet, P. ; Salmeron, M. *Phys. Rev. B.* **1997**, 56, 15885.

28. Cerdá, J. ; Yoon, A. ; Van Hove, M.A. ; Sautet, P. ; Salmeron, M. et al. *Phys. Rev. B.* **1997**, 56, 15900.

29. http://www.icmm.csic.es/jcerda

30. Cerdá, J.; Soria, F. *Phys. Rev. B*. **2000**, 61, 7965.

31. Janta-Polczynski, B.A.; Cerdá, J.I.; Ethier-Majcher, G.; Piyakis, K; Rochefort, A.; *J. Appl. Phys.* **2008**, 104,23703.

32. Tatarkhanov, M.; Fomin, E.; Salmeron, M.; Andersson, K.; Ogasawara, H.; Pettersson, L.G.M.; Nilsson, A.; Cerda, J. *J. Chem. Phys.***2008**, 129, 154109.

33. http://stm.lbl.gov/Salmeron_group/vt2.html

34. Gsell, M.;. Jakob, P.; Menzel, D.*Science,* **1998***,* 280.)

35. An detailed account of the formation and orientation of stripes on Ru(0001) will be presented separately. Maier, S.; Stass, I.; Salmeron, M. In preparation **2009**.

36. Clay, C.; Haq, S.; Hodgson, A. *Phys. Rev. Lett*. **2004**, 92.

37. Andersson, K.; Nikitin, A.; Pettersson, L.G.M.; Nilsson, A.; Ogasawara, H. *Phys. Rev. Lett.* **2004**, 93, 196101.

38. Haq, S.; Clay, C.; Darling,G.R.; Zimbitas, G.; Hodgson, A.; *Phys. Rev. B.* **2006**, 7**3**, 115414.

39. Faradzhev, N.S.; Kostov, K.L.; Feulner, P.; Madey,.E.; Menzel, D.Chem. *Phys. Lett*. **2005**, 415,

40. Ranea,V.A.; Michaelides, A.; Ramirez, R; de Andres, P.L.; Verges, J.A.; King, D.A.; *Phys. Rev. Lett*. **2004**, 92, 136104.

41. Michaelides, A.; Ranea,V.A.; de Andres, P.L.;. King, D.A. *Phys. Rev. Lett*. **2003**, 90, 216102.

42. Meng, S.; E.G. Wang, E.G.; Gao, S. *Phys Rev. B.* **2004**, 69.